



24

25 **Abstract**

26 Human pluripotent stem cells (hPSCs) are an important system to study early human  
27 development, model human diseases, and develop cell replacement therapies. However, genetic  
28 manipulation of hPSCs is challenging and a method to simultaneously activate multiple genomic  
29 sites in a controllable manner is sorely needed. Here, we constructed a CRISPR-ON system to  
30 efficiently upregulate endogenous genes in hPSCs. A doxycycline (Dox) inducible  
31 dCas9-VP64-p65-Rta (dCas9-VPR) transcription activator and a reverse Tet transactivator (rtTA)  
32 expression cassette were knocked into the two alleles of the *AAVS1* locus to generate an iVPR  
33 hESC line. We showed that the dCas9-VPR level could be precisely and reversibly controlled by  
34 addition and withdrawal of Dox. Upon transfection of multiplexed gRNA plasmid targeting the  
35 *NANOG* promoter and Dox induction, we were able to control *NANOG* gene expression from its  
36 endogenous locus. Interestingly, an elevated *NANOG* level did not only promote naïve pluripotent  
37 gene expression but also enhanced cell survival and clonogenicity, and it enabled integration of  
38 hESCs with the inner cell mass (ICM) of mouse blastocysts *in vitro*. Thus, iVPR cells provide a  
39 convenient platform for gene function studies as well as high-throughput screens in hPSCs.

40

41

42

## 43 **Introduction**

44 Human pluripotent stem cells (hPSCs), including human embryonic stem cells (hESCs) and  
45 human induced pluripotent stem cells (hiPSCs), are capable of self-renewal indefinitely and have  
46 the potential to differentiate into all cell types in the human body. Therefore this system offers a  
47 useful platform to study early human embryogenesis and a potential cell source for regenerative  
48 medicine. Moreover, functional cells derived from hESCs can be used to model human diseases in  
49 the context of drug toxicity tests and new drug development. These applications rely on methods  
50 to precisely control gene expression. However, because of difficulties in culture and transfection,  
51 targeted regulation of gene expression in hPSCs remains a technically challenging task. A method  
52 for efficient, rapid, and controllable gene activation is sorely needed.

53 Recently, the clustered regularly interspaced short palindromic repeat (CRISPR)/Cas9 system  
54 emerged as a powerful and versatile tool for genome editing (Wiedenheft et al. 2012). CRISPR  
55 was initially discovered as the adaptive immune system of bacteria and archaea (Wiedenheft et al.  
56 2012). In response to viral and plasmid infection, bacteria and archaea could cut and degrade the  
57 foreign DNA recognized by a matching spacer RNA with the help of the Cas9 enzyme  
58 (Wiedenheft et al. 2012). CRISPR was rapidly transformed to a genome editing tool, and it has  
59 been shown to work in a wide range of systems, from plants to human cells, since the Cas9  
60 nuclease can be directed easily to virtually anywhere in the genome using a short guide RNA and  
61 cutting the target DNA (Hsu et al. 2014). In pluripotent stem cells, the CRISPR system has been  
62 used to perform highly efficient gene knock-out and knock-in studies (Hsu et al. 2014). In addition  
63 to genome editing, a nuclease inactivated Cas9 (dCas9) was developed (Gilbert et al. 2014). By  
64 fusing dCas9 with transcription activators and repressors, such as VP64, and KRAB (Balboa et al.  
65 2015; Gilbert et al. 2014; Mandegar et al. 2016; Genga et al. 2015), or with epigenetic modifiers,  
66 such as the catalytic domain of acetyltransferase p300 (Hilton et al. 2015) and Tet (ten eleven  
67 translocation) dioxygenase (Xu et al. 2016), one can use the CRISPR system to activate or inhibit  
68 gene expression or modify the histone and DNA methylation status at the desired locus.

69 Because of its potential applications in regenerative medicine, random insertion of foreign DNA  
70 into the genome of hPSCs should be avoided, since this may cause harmful mutations. The  
71 Adeno-Associated Virus Integration Site 1 (*AAVSI*) locus resides in the first intron of the  
72 *PPP1R12C* gene and has been used as a safe harbor for transgene integration (Smith et al. 2008;  
73 Hockemeyer et al. 2009; Lombardo et al. 2011; Qian et al. 2014; Zhu et al. 2014; Genga et al.  
74 2015). Here we generated an iVPR hESC line by knocking-in the inducible dCas9-VPR system

75 into the two alleles of the *AAVSI* locus. Detailed characterization of the iVPR hESC demonstrated  
76 that dCas9-VPR protein could be induced by Dox within 12 hours and disappear after Dox  
77 withdrawal. An inducible *NANOG* overexpression line (iNANOG) was established based on the  
78 iVPR system. We found a significant increase in NANOG protein after Dox induction. INANOG  
79 cells upregulated naïve pluripotency genes and were able to grow for a significant length of time in  
80 a naïve state medium containing ERK and GSK3 inhibitors and human LIF. The iVPR system can  
81 be a valuable system to control gene expression from endogenous loci and serve as platform for  
82 genome wide screens to identify new genes that can regulate stem cell self-renewal and  
83 differentiation.

84

## 85 **Results**

### 86 **DCas9-VPR mediated robust ectopic and endogenous gene activation in human cell lines**

87 To construct a robust and tunable gene activation system in hPSCs, we first compared the  
88 activation efficiency of dCas9-VPR (Chavez et al. 2015) with dCas9-VP64 (Kearns et al. 2014)  
89 and the Doxycycline (Dox) inducible Tet-On transactivator (rtTA) (Fig. 1A). We constructed  
90 plasmids to express gRNA targeting the TetO sequence (gTetO), and tested the ability of  
91 dCas9-VPR+gTetO or dCas9-VP64+gTetO to activate the synthetic TRE promoter driving  
92 enhanced blue fluorescent protein expression (TRE-BFP) in 293FT cells (Fig. 1A). The Tet  
93 transactivator (rtTA) was used as positive control (Fig. 1B). DCas9-VPR strongly activated BFP  
94 fluorescence, 43.1% of cells were BFP positive, while in the rtTA+Dox and dCas9-VP64 groups,  
95 only 28.2% and 5.8% of cells activated BFP, respectively (Fig. 1C and D). Moreover, dCas9-VPR  
96 resulted in the strongest mean BFP fluorescence intensity, indicating that it is the strongest  
97 activator among the three (Fig. 1D).

98 We next tested the dCas9-VPR function in hESCs. DCas9-VPR, gTetO, and TRE-BFP  
99 plasmids were co-transfected into H9 hESCs. In another group, rtTA and TRE-BFP plasmids were  
100 co-transfected. FACS analysis showed that nearly 17% of cells in the dCas9-VPR group turned on  
101 BFP, while 24.7% of cells in the rtTA group were BFP positive after Dox induction, and only 0.6%  
102 of cells exhibited BFP fluorescence without Dox (Fig. 1E). Interestingly, the dCas9-VPR group  
103 showed the strongest mean fluorescence intensity (Fig. 1F). This is consistent with our result based  
104 on 293FT cells and proves that dCas9-VPR is a robust transcription activator, even compared with  
105 rtTA. We also tested the activation effect of dCas9-VPR in mouse embryonic stem cells (mESCs)  
106 and mouse embryonic fibroblasts (MEFs) and obtained similar results (Fig. S1A and B).

107 We then tested the efficiency of dCas9-VPR to activate normally silenced pluripotency genes  
108 in human cells. Two gRNAs targeting the -254 and -144 positions upstream of the transcription  
109 start site (TSS) of the pluripotency gene *NANOG* were selected (Fig. 2A). A GFP-2A-Puromycin  
110 resistant gene expression cassette was placed after the gRNA cassette both to monitor the  
111 transfection efficiency and for selection (Fig. 2A). *NANOG* cannot be activated by gNANOG  
112 alone or by dCas9-VPR together with the control gTetO. However, introducing gNANOG and  
113 dCas9-VPR together could elevate the *NANOG* transcript level by up to 150-fold in 293FT cells,  
114 indicating that it has a robust gene activation function (Fig. 2C).

115 Next, we tested whether the dCas9-VPR system could simultaneously activate multiple genes  
116 in human cells, we designed 2 different gRNAs per gene promoter for *HOXA10*, *SNAIL1*, *MESPI*,  
117 *GATA5* and *HOXA9*. First we tested the activation efficiency of these gRNAs towards their target  
118 genes when transfected separately in 293FT cells (Fig. 2D). Q-PCR analysis showed all of the five  
119 pairs of gRNAs can activate their target gene upon co-transfection with dCas9-VPR (Fig. 2D). We  
120 next pooled gRNA pairs of two genes (2×gRNAs: *MESPI*, *GATA5*), three genes (3×gRNAs:  
121 *HOXA10*, *SNAIL1*, *HOXA9*) or five genes (5×gRNAs: *HOXA10*, *SNAIL1*, *MESPI*, *GATA5* and  
122 *HOXA9*) to test the co-activation efficiency. Upon co-transfection with dCas9-VPR, different  
123 combination of gRNAs upregulated their target genes together (Fig. 2E), indicating that  
124 dCas9-VPR system could be a useful tool for multiplexed endogenous gene activation.

125 To validate the utility of the dCas9-VPR system in hESCs, we transfected H9 hESCs with  
126 either dCas9-VPR and gNANOG or with rtTA and *NANOG* coding DNA sequence (CDS) joined  
127 to H2B-mCherry through a 2A peptide driven by a TRE promoter. As shown in Fig. 3A, for the  
128 dCas9-VPR group, increased NANOG protein expression (in red) can be detected in colonies with  
129 GFP fluorescence. Upon Dox induction, stronger NANOG was also visible in Tet-On system  
130 transfected cells and co-localized with the H2B-mCherry (Fig. 3A). Quantitative PCR (Q-PCR)  
131 and western blot confirmed the elevated NANOG level induced by either dCas9-VPR+gNANOG  
132 or *NANOG* CDS. The transcript level of another pluripotency marker gene, *OCT4*, was increased  
133 synergistically (Fig. 3B). Western blot analysis confirmed the upregulation of NANOG and OCT4  
134 proteins in transiently transfected H9 cells (Fig. 3C). We generated a transgenic hESC line  
135 constitutively expressing dCas9-VPR and observed no cytotoxicity, decrease in pluripotency gene  
136 expression, or change in cell morphology for long-term cultures (Fig. 3D and E). This suggests  
137 that the dCas9-VPR system is suitable for gene activation studies in hPSCs.

138

139

## 140 **Generation of an inducible idCas9-VPR hESC knock-in line**

141 To achieve efficient, tunable, and reversible gene activation while avoiding compromising the  
142 genome integrity of hPSCs, we engineered an iVPR system by inserting the CAG promoter driving  
143 the rtTA expression cassette and the TRE promoter driving the dCas9-VPR cassette into the two  
144 alleles of the *AAVSI* locus on chromosome 19. H9 hESCs were co-transfected with two donor  
145 plasmids containing dCas9-VPR and M2rtTA, as well as a pair of Cas9 nickase plasmids with  
146 *AAVSI* targeting gRNAs to induce DNA double-strand break (DSB) and homology recombination  
147 (HR) (Fig. S2A). After puromycin and neomycin double selection for 2 weeks, we picked and  
148 expanded 17 clones. Upon addition of Dox, all the clones showed clear induction of dCas9-VPR  
149 protein expression (Fig. S2B). Genomic DNA PCR was performed to select correct targeted clones  
150 and rule out random insertions (Fig. S2C). Clone 2, 6 and 8 had targeted insertion at both *AAVSI*  
151 alleles and without any random insertion (Fig. S2C). They were chosen for further analysis.  
152 Southern blot confirmed that in all three clones, both alleles of *AAVSI* contained the correct  
153 insertion (Fig. 4A and B). Q-PCR analysis showed that in hESCs, without Dox treatment, little  
154 *dCas9-VPR* transcript could be detected, while after Dox addition, strong *dCas9-VPR* expression  
155 was induced (Fig. 4C). Karyotype analysis showed that all three clones had normal 46XX karyotype  
156 (Fig. S2D). iVPR clone 2 was chosen for further study. Without Dox, we could not detect any  
157 dCas9-VPR protein in iVPR cells. The dCas9-VPR protein appeared after 12 hours of Dox addition  
158 and reached a plateau at 24 hours (Fig. 4D). While 6 hours after Dox withdrawal, the dCas9-VPR  
159 protein decreased, by 12 hours, it decreased to a low level and could not be detected anymore after  
160 24 hours (Fig. 4D). The induction of dCas9-VPR from the *AAVSI* locus was not affected by  
161 differentiation. We induced mesoderm differentiation by culturing cells in an RPMI medium  
162 supplemented with albumin, ascorbic acid, transferrin, selenite, BMP4 (5ng/ml) and CHIR99021 (2  
163  $\mu$ M) as described by Burridge et al. (Burridge et al. 2015). Q-PCR analysis showed that after 3 days  
164 of differentiation, pluripotency marker genes *OCT4* and *SOX2* were significantly downregulated,  
165 while *dCas9-VPR* was highly expressed as long as Dox was present, regardless whether cells were  
166 in hESC culture medium E8 or in the differentiation medium (Fig. 4E). Genes related to mesoderm  
167 differentiation and epithelial to mesenchymal transition, such as *SNAIL*, were strongly upregulated  
168 by BMP4 and CHIR99021, confirming that hESCs had taken a mesoderm fate (Fig. 4E). These  
169 results suggest that the iVPR hESC line can be used for efficient and reversible gene activation.

170

## 171 **Upregulation of *NANOG* by dCas9-VPR promoted naïve state of pluripotency**

172 The iVPR system provided a unique platform to investigate gene functions through activation  
173 from the endogenous locus. *NANOG* is a key regulator of pluripotency. We generated iNANOG  
174 hESCs by transfecting the PiggyBac based gNANOG plasmid described earlier into iVPR clone 2, 6,  
175 and 8, followed by FACS selection of GFP<sup>+</sup> cells. Q-PCR analysis showed that after 2 days of Dox  
176 treatment, only iNANOG cells showed a significant increase (about 18 folds) in the *NANOG* mRNA  
177 level, while iVPR cells, with or without Dox, or iNANOG cells without Dox did not show any  
178 change in *NANOG* expression, indicating that the iNANOG system is tightly regulated (Fig. 5A).  
179 We also tested the time window of *NANOG* down-regulation after Dox withdrawal. *NANOG* mRNA  
180 was unchanged during the first 12 hours and decreased after 24 hours. It approached the background  
181 level after 48 hours (Fig. 5B). We next examined the change in NANOG protein level after Dox  
182 addition and withdrawal. Western blot revealed that dCas9-VPR protein became detectable 12 hours  
183 after Dox induction and reached a significant level after 24 hours (Fig. 5C, dCas9, long exposure;  
184 LE). Accordingly, NANOG protein showed an obvious increase after 24 hours and maintained at  
185 high level as long as dCas9-VPR was present (Fig. 5C, NANOG, LE). On the other hand, 6 hours  
186 after Dox removal, the dCas9-VPR protein decreased significantly (Fig. 5D, dCas9, short exposure;  
187 SE). The decline of the dCas9-VPR protein was most apparent during the first 24 hours. After 4 days  
188 without Dox, dCas9-VPR protein became almost undetectable (Fig. 5D). Similarly, the NANOG  
189 protein level dropped to the background level after 4 days of Dox withdrawal (Fig. 5D). Q-PCR  
190 analysis showed that after Dox induction, iNANOG significantly upregulated naïve state related  
191 genes such as *OCT4*, *PRDM14*, *GDF3*, and *LEFTYB*, while the early differentiation genes such as  
192 *AFP* was significantly downregulated (Fig. 5E). *XIST*, a long non-coding RNA involved in X  
193 chromosome inactivation were also downregulated after *NANOG* induction (Fig. 5F). The  
194 expression of SSEA3, a more rigorous pluripotency cell surface marker, was increased and became  
195 more homogeneous after *NANOG* elevation (Fig. 5G and Fig. S3). In addition to elevated expression  
196 of pluripotency genes, iNANOG cells also showed enhanced survival and proliferation abilities.  
197 Clonogenicity assay showed that after Dox induction, twice as many clones formed from dissociated  
198 iNANOG single cells (Fig. 5H and I). Finally, we tested whether *NANOG* upregulation by iVPR  
199 may facilitate hESCs to enter the naïve state of pluripotency. iVPR cells and iNANOG cells were  
200 cultured in 2iL medium which supplemented with ERK inhibitor PD0325901, GSK3 inhibitor  
201 CHIR99021, human LIF, and bFGF proteins with or without Dox addition (Silva et al. 2009;  
202 Takashima et al. 2014). Upon changing to the 2iL medium, hESCs colonies changed into a  
203 domed-shaped morphology and became more compact (Fig. 5J and K). iNANOG cells without  
204 induction can only survive for no more than three passages in the 2iL medium (Fig. 5J). Interestingly,  
205 Dox induced iNANOG cells can grow in the 2iL medium for longer than 9 passages with single cell

206 dissociation and a 1:15 passage ratio (Fig. 5J and K). In contrast to iNANOG cells, Dox treated  
207 iVPR cells could not survive in 2iL conditions (Fig. 5J). Thus, upregulation of *NANOG* from its  
208 endogenous locus significantly improved single cell clonogenicity and permitted hESCs to grow in a  
209 naïve state culture environment.

210

### 211 **Upregulation of *NANOG* enabled hESCs to integrate with mouse ICM *in vitro***

212 Entering the pluripotent ICM lineage is considered a more stringent test for naïve state ESCs  
213 (Gafni et al. 2013; Takashima et al. 2014). We next used *in vitro* human–mouse blastocyst chimera  
214 assay to assess the functionality of iNANOG cells (Fig 6A). To exclude the influence of Dox  
215 treatment only, wild type hESCs stably carrying gNANOG (WTSG) were used as the control. For  
216 this series of experiments, we also added Forskolin (a cAMP agonist) into the 2iL medium, since it  
217 had been shown to promote hPSCs to enter the naïve state (Hanna et al. 2010; Ware et al. 2014;  
218 Duggal et al. 2015). We refer to this medium as 2iL/FK. iNANOG cells showed further enhanced  
219 proliferation in the 2iL/FK medium and were able to form large, dome-shaped colonies (Fig. 6B),  
220 while cells without *NANOG* overexpression could only form small colonies (Fig. S4A). E3.5  
221 blastocysts were collected from ICR mice for hESC injection. iNANOG cells and WTSG cells  
222 cultured with or without Dox, in either the E8 or 2iL/FK medium, were dissociated into single  
223 cells. 10–15 single cells were injected into the blastocoel cavity and cultured in a 1:1 mixed  
224 KSOM:2iL/FK medium for 24 hours (Fig. 6A). Because cells without *NANOG* overexpression  
225 only formed small colonies on feeder in the 2iL/FK medium, we could not obtain sufficient pure  
226 hESCs for blastocyst injection. Therefore, this group was omitted from this series of experiments.  
227 Since all cells used for injection contained GFP transgene expressed from the gNANOG plasmid,  
228 the location of human cells in the mouse blastocysts could be followed directly under the  
229 fluorescence microscope. 4–6 hours after injection, most blastocysts contained GFP positive  
230 human cells (Fig. 6B and C). After 24 hours of culture, many embryos still contained hESCs (Fig.  
231 6B). We used time-lapse imaging to monitor the activity of hESCs in mouse blastocysts over time  
232 (Supplementary movie S1). Interestingly, endogenous *NANOG* overexpression strongly enhanced  
233 the survival of hESCs in mouse blastocysts. 12 hours after injection, 2iL/FK cultured Dox induced  
234 gNANOG cells could be found in approximately 82% of blastocysts, while E8 cultured Dox  
235 induced gNANOG cells were alive in 73% of blastocysts (Fig. 6C and S4B). In contrast, without  
236 Dox induction, E8 cultured iNANOG cells could only be seen in 49% of injected blastocysts (Fig.  
237 6C and S4B). We next analyzed the locations of the transplanted hESCs. Injected embryos were  
238 fixed after 24 hours of culture, stained with CDX2 (a trophectoderm marker) and  $\beta$ -Catenin, and

239 observed with a confocal microscope. Different integration patterns were shown: hPSCs integrated  
240 into the ICM region (ICM), in both the ICM and the trophectoderm (Multiple), only in the  
241 trophectoderm (TE), and disappeared (None) (Fig. 6D). We also performed live imaging to  
242 monitor the behavior of iNANOG cells in the mouse blastocyst. Interestingly, 2iL/FK cultured  
243 iNANOG cells tend to migrate with mouse inner cell mass cells as blastocyst hatching from the  
244 zona pellucida (Fig. 6E). *NANOG* overexpression significantly improved the percentage of cells  
245 remaining in blastocysts, and the 2iL/FK culture further increased the ICM integration proportion  
246 (Fig. 6F, G, and S4C). On average, two 2iL/FK or E8 cultured iNANOG cells could be found in  
247 the ICM region 24 hours after injection, while without *NANOG* overexpression, hardly any GFP  
248 cells were seen in the ICM (Fig. 6G). Thus, upregulation of *NANOG* from its endogenous locus  
249 greatly enhanced cell survival and their subsequent ICM integration in hPSC-mouse blastocyst  
250 chimeras.

251

## 252 **Discussion**

253 In this study, we generated an inducible CRISPR-ON hESC line by targeting the *AAVS1* locus.  
254 Based on both our results and those of Chavez et al. (Chavez et al. 2015), dCas9-VPR appeared to  
255 be a stronger activator than VP64 to induce gene expression from both ectopic and endogenous  
256 promoters. It even led to a higher level of reporter gene activation compared with Tet-ON rtTA,  
257 where VP64 was fused with Tet protein directly bound to the TRE elements. This is likely due to  
258 the combined effects of VP64, NF- $\kappa$ B transactivating subunit p65, and the viral transcription  
259 factor Rta, which together can recruit a multitude of endogenous factors to achieve dramatically  
260 enhanced transcriptional activation. Other dCas9 based transcription activators have been  
261 generated. For example, Balboa et al. found increased activation ability with more VP16 fusing  
262 together. Using the longest version of dCas9-VP192 combined with inducible systems, they  
263 successfully facilitated human cell reprogramming and differentiation (Balboa et al. 2015).  
264 Konermann et al. engineered a structure-guided CRISPR synergistic activation mediator system  
265 (SAM), where they engineered gRNA2.0 by replacing the tetraloop and stem loop 2 of the original  
266 gRNA with a minimal hairpin aptamer that specifically binds to MS2 bacteriophage coat proteins  
267 (Konermann et al. 2014). By co-expression of dCas9-VP64, gRNA2.0, and MS2 fused with p65  
268 and the activation domain of the human heat-shock factor 1 (HSF1), highly effective gene  
269 activation can be achieved (Konermann et al. 2014). Tanenbaum et al. constructed a SunTag  
270 system: dCas9 was joined with 10 copies of GCN4 peptide (SunTag), while VP64 was fused with  
271 scFv-GCN4 (the single-chain variable fragment (scFv) antibody of GCN4) (Tanenbaum et al.

272 2014). When co-expressed in the cell, SunTag was bound by scFv-GCN4, and multiple copies of  
273 VP64 resulted activation of the target gene (Tanenbaum et al. 2014). Compared with the systems  
274 discussed above, which required introducing tandem repeat large cassette or the co-expression of  
275 two components in addition to the gRNA, dCas9-VPR is a simple and effective option.

276

277 In our study, we chose to insert the iVPR system into the *AAVSI* locus, since it has been used as a  
278 ‘safe harbor’ for transgene insertion in human stem cell systems (Dekelver et al. 2010). For  
279 example, Genga et al. constructed a GFP labeled H1 hESC line by knocking-in a CAG-GFP into the  
280 *AAVSI* locus. Besides, an inducible dCas9-KRAB gene inhibition system was also introduced into  
281 the GFP-H1 cells. By infecting sgRNA targeting the exogenous CAG promoter, they successfully  
282 realized CRISPR based inhibition of exogenous gene in hESCs (Genga et al. 2015). González et  
283 al. inserted the Dox inducible Cas9 system into the 2 alleles of the *AAVSI* locus of HUES8 hESCs  
284 (González et al. 2014; Zhu et al. 2014; Zhu et al. 2015). The resulting iCRISPR hESC line enabled  
285 selection-free gene knock-out and the generation of lineage-specific knock-in reporters. This  
286 demonstrated that when Cas9 was expressed in a controllable manner from a suitable locus, the  
287 resulting cell line can be a powerful platform for genome editing in normally hard to transfect  
288 human stem cells (Zhu et al. 2015). Similarly, using the iVPR line, we found that the efficiency to  
289 generate an iNANOG line was much improved. Upon Dox addition and withdrawal, *NANOG*  
290 transcripts and proteins could be up- and down-regulated in a highly repeatable manner, which  
291 greatly facilitated downstream experiments. Recently, Ordovás et al. reported *AAVSI*-locus  
292 mediated transgene inhibition in hESCs, and that inhibition may due to different cassettes inserted  
293 into the locus (Ordovás et al. 2015). We tested the iVPR expression in both undifferentiated hESCs  
294 and after induction of mesoderm differentiation. The level of *dCas9-VPR* transcripts was even  
295 higher upon Dox treatment after mesoderm induction (Fig. 4E). The iVPR and iNANOG cells  
296 have been maintained for more than 6 months, and we did not observe any reduction in the level of  
297 *dCas9-VPR* or *NANOG* induced by Dox. Thus, results us and other groups suggested that, in most  
298 cases, *AAVSI* locus integration is a reliable approach to generate transgenic hPSCs.

299

300 *NANOG* is a master transcription factor for pluripotency in both human and mouse ESCs (Mitsui  
301 et al. 2003; Boyer et al. 2005; Chambers et al. 2007). During somatic cell reprogramming to  
302 pluripotent stem cells, ectopic expression of *NANOG* helped to speed up reprogramming and  
303 restrict partially reprogrammed cells to the ground state (Hanna et al. 2009; Silva et al. 2009).  
304 Different from mESCs, conventional cultured hESCs are in a primed state, similar to the epiblast

305 stem cells in mice (Brons et al. 2007; Tesar et al. 2007). Recently, multiple groups reported  
306 methods to obtain naïve state hPSCs that resemble ground-state mESCs (Gafni et al. 2013; Duggal  
307 et al. 2015; Takashima et al. 2014; Theunissen et al. 2014). Takashima et al. showed that ectopic  
308 expression of *NANOG* and *KLF2* could reset the self-renewal requirements of hPSCs so that they  
309 can be grown in a medium containing ERK1/2 inhibitor PD0325901 and GSK3 inhibitor  
310 CHIR99021, and adopt a domed-shaped morphology similar to that of mESCs (Takashima et al.  
311 2014). Here we increased the expression of endogenous *NANOG* by targeting a strong  
312 transcription activator, dCas9-VPR, to its promoter. As expected, we observed upregulation of  
313 naïve state genes such as *GDF3*, *PRDM14*, and *LEFTYB* and downregulation of early  
314 differentiation gene *AFP*. Interestingly, these iNANOG cells showed a significantly improved  
315 survival ability and clonogenicity when cultured in the primed state, and they could grow in 2i  
316 plus LIF conditions for more than nine passages. The improved survival and self-renewal of  
317 iNANOG cells was not due to the effect of Dox treatment as described by Chang et al. (Chang et al.  
318 2014), because Dox treated iNANOG cells showed significantly higher clonogenicity over Dox  
319 treated iVPR cells (Fig. 5H and I). The enhanced survival ability seemed to have a significant  
320 influence on whether hPSCs can integrate with the ICM of mouse blastocysts during *in vitro*  
321 culture. We found that even when iNANOG cells were in the primed state, after injection into  
322 mouse blastocysts, more cells remained inside the blastocysts and some of the cells were able to  
323 integrate with mouse ICM cells (Fig. 6F and G). Culturing iNANOG cells in 2iL/FK naïve state  
324 medium (Duggal et al. 2015) further improved the ICM integration rate (Fig. 6F and G). iNANOG  
325 cells displayed highly dynamic interactions with mouse ICM cells, as observed in time-lapse  
326 movies (Supplementary movie S1). They migrated with mouse ICM cells as blastocysts hatched  
327 from zona pellucida. However, despite enhanced survival ability of iNANOG cells, many injected  
328 cells died over time. After 24 hours, more than 30% of injected blastocysts lost all iNANOG cells  
329 and more than 60% of blastocysts lost the injected hESCs if *NANOG* was not overexpressed (Fig.  
330 6F). This was partially caused by poor survival of hESCs in the IVC1 and -2 media designed to  
331 culture peri-implantation mouse and human embryos (Bedzhov and Zernicka-Goetz 2014;  
332 Deglincerti et al. 2016; Shahbazi et al. 2016) (Fig. S4D). Thus, to achieve better naïve hPSC and  
333 mouse ICM integration, a culture medium suitable for both mouse blastocysts and hPSCs may be  
334 needed. The effect of *NANOG* overexpression on cell survival and self-renewal is also in  
335 accordance with the observation that chromosome 12, where the *NANOG* gene is located, is the  
336 most frequently gained chromosome in culture adapted hPSCs (Baker et al. 2007) and during  
337 hiPSC generation (Taapken et al. 2011). Moreover, *NANOG* was reported to be upregulated by a  
338 number of factors such as *STAT3*, Hedgehog signaling, hypoxia, etc., in human cancers, and

339 repression or ablation of *NANOG* inhibited tumor initiation (Gong et al. 2015). Thus, iNANOG  
340 hESCs, where the endogenous *NANOG* can be activated by dCas9-VPR in a controllable manner,  
341 may also be a good system to study the process of hPSC adaptation and cancerous transformation.

342

343 In summary, the iVPR hESC line generated and characterized in this study offered a convenient,  
344 stable, and highly controllable platform for gene activation studies. It can also be used to  
345 investigate the function of regulatory elements in the genome such as super enhancers as well as  
346 for genome wide screens using established human gRNA libraries.

347

## 348 **Methods**

### 349 **HESC culture**

350 H9 hESCs (WiCell Institute) were maintained on inactivated mouse embryonic fibroblast (MEF)  
351 cells in standard hESC medium consisting of KO-DMEM (Invitrogen) supplemented with  
352 1×Nonessential Amino Acids (NEAA) (Invitrogen), 0.1 mM 2-mercaptoethanol (Sigma-Aldrich), 1  
353 mM GlutaMAX (Invitrogen), 20% Knock-out serum-replacement (KOSR) (Invitrogen) and 4 ng/ml  
354 bFGF (Peprotech). Cells were cultured at 37 °C in a humidified atmosphere with 5% CO<sub>2</sub> in air.  
355 They were passaged with 1 mg/ml collagenase IV (Invitrogen) and seeded onto MEFs. For  
356 feeder-free culture, hESCs were grown for more than three passages on Matrigel (growth factor  
357 reduced, BD Biosciences) in the absence of feeders in E8 medium (Invitrogen).

358

### 359 **Plasmid construction**

360 dCas9-VPR was constructed by fusing the nuclease deficient Cas9 (dCas9) with transcription  
361 activator VP64, p65, and Rta in tandem as described by Chavez et al. (Maeder et al. 2013). For  
362 constitutive expression, dCas9-VPR was placed behind a CAG promoter in a PiggyBac vector also  
363 containing a PGK promoter driving a hygromycin resistance gene. For inducible expression from  
364 the *AAVS1* locus, dCas9-VPR was placed behind a TRE promoter in the *AAVS1* homologous  
365 recombineering donor plasmid, as shown in Fig. S2A. dCas9-VP64 was constructed by fusing  
366 dCas9 with VP64. Tet-On system was obtained from Clontech (<http://www.clontech.com>).  
367 PiggyBac plasmids were generous gift from the Sanger institute, Cambridge, UK  
368 (<http://www.sanger.ac.uk>). The multiple *NANOG* gRNA expression plasmid was constructed by  
369 SynGene (<http://syngen.tech>) as depicted in Fig. 2A.

370

### 371 **Naïve state culture condition for hPSCs**

372 For naïve state conversion, cells cultured in standard hESC medium on MEFs were dissociated to  
373 single cells using 0.05% trypsin/EDTA solution (Invitrogen), replated on MEFs, and cultured  
374 overnight in standard hESC medium supplement with 10  $\mu$ M Rho Kinase (ROCK)-inhibitor  
375 Y-27632 (Calbiochem). The next day, the standard medium was changed to the 2iL or 2iL/FK (for  
376 injection) medium, which consisted of KO-DMEM (Invitrogen), 20% KOSR, 1 $\times$ NEAA, 0.1 mM  
377 2-mercaptoethanol, 1 mM GlutaMAX, 12 ng/ml bFGF, 10 ng/ml human recombinant LIF  
378 (Peprotech), 1  $\mu$ M ERK1/2 inhibitor PD0325901 (Peprotech), 3  $\mu$ M GSK3 inhibitor CHIR99021  
379 (Peprotech), 10  $\mu$ M Forskolin (Peprotech), and 50  $\mu$ g/ml ascorbic acid (Sigma). HESCs changed to  
380 a dome-shaped morphology within 4–6 days after culturing in the 2iL or 2iL/FK medium and were  
381 passaged every 4 days as single cells using 0.05% trypsin/EDTA.

382

### 383 **Cardiac mesoderm differentiation from hESCs**

384 For cardiac mesoderm differentiation, hESCs maintained on Matrigel (growth factor reduced, BD  
385 Biosciences) in E8 were dissociated into single cells with Accutase (Invitrogen), then seeded onto  
386 Matrigel-coated tissue culture dishes at a density of  $5 \times 10^4$  cells/cm<sup>2</sup> and cultured in E8 for 3 days.  
387 Then the medium was switched to the RPMI1640 medium supplemented with Albumin, Ascorbic  
388 acid, transferrin, selenite, 5 ng/ml BMP4 (R&D Systems), and CHIR99021 to induce cardiac  
389 mesoderm formation.

390

### 391 **Quantitative PCR**

392 Total RNA was extracted with TRIZOL (Invitrogen). 1  $\mu$ g RNA of each sample was used for reverse  
393 transcription with Superscript III (Invitrogen). Q-PCR reactions were performed using GoTaq qPCR  
394 Master Mix (Promega) in a CFX96 Real-Time System (Bio-Rad). The relative expression level of  
395 each gene was normalized against the Ct (Critical Threshold) value of the house-keeping gene  
396 *GAPDH* using the Bio-Rad CFX Manager program. Primer sequences are listed in table S2.

397

### 398 **Antibodies, immunostaining, western blot, and FACS analysis**

399 For immunostaining, cells were fixed in 4% paraformaldehyde (PFA) in PBS, permeabilized in  
400 0.5% Triton X-100 (Sigma), blocked in 5% normal goat serum (Origene) and incubated with  
401 primary antibodies against NANOG (1:200), SSEA3 (1:200) in 4 °C overnight and detected by  
402 DyLight 488- or 549-conjugated secondary antibodies (Thermo). Nuclei were stained with DAPI  
403 (Sigma). A Nikon Ti-U fluorescence microscope was used for image acquisition. For western blot,

404 cells were lysed in a RIPA buffer (Applygen, <http://applygen.com.cn>) with Protease Inhibitor  
405 Cocktail (Roche). Total proteins were separated on a 12% SDS/PAGE gel, transferred to  
406 nitrocellulose membrane (Whatman). The membrane was blocked with 5% non-fat dry milk in  
407 TBST and then incubated with primary antibodies against Cas9 (Genetex, 1:1000), GAPDH  
408 (CWBio, 1:1000), OCT4 (Santa Cruz, 1:1000) and NANOG (Cell Signaling Technology, 1:1000).  
409 After washing, the membrane was incubated with anti-mouse or anti-rabbit peroxidase-conjugated  
410 secondary antibodies (ZSGB-Bio <http://www.zsbio.com/>). Bands recognized by antibodies were  
411 revealed by ECL reagent (Pierce). For FACS analysis, cells were first dissociated with 0.05%  
412 Trypsin in 0.2% EDTA and PBS. FACS was performed on a Fortessa flow cytometer (Becton  
413 Dickinson).

414

#### 415 **Mouse blastocyst injection and in vitro culture**

416 Mouse morula were collected from ICR females 2.5 days post-coitus and cultured in KSOM  
417 medium (95mM NaCl, 2.5mM KCl, 0.35mM KH<sub>2</sub>PO<sub>4</sub>, 0.2mM MgSO<sub>4</sub>·7H<sub>2</sub>O, 0.2mM glucose,  
418 10mM sodium lactate, 25mM NaHCO<sub>3</sub>, 0.2mM sodium pyruvate, 1.71mM CaCl<sub>2</sub>·2H<sub>2</sub>O, 0.01mM  
419 EDTA, 1mM L-glutamine, 0.1mM EAA, 0.1mM NEAA, 4mg/ml BSA) at 37°C , 5%CO<sub>2</sub> for 24  
420 hours to get blastocysts. HESCs were briefly treated with Accutase for single cell and injected  
421 (~10-15 cells for each embryo) on a Nikon microscope fitted with piezo-driven Eppendorf NK2  
422 micromanipulator, CellTram air and CellTram Vario. After injection, embryos containing hESCs  
423 were cultured in medium supplemented with naïve culture medium :KSOM (1:1) (Chen et al. 2015)  
424 in 37 °C, 5% CO<sub>2</sub> incubator. After injected embryos reformed blastocoel, the chimera embryos  
425 were live cell imaged using Leica microscope fitted with a live cell imaging system and fixed after  
426 24-36 hours post-injection for staining and confocal imaging. For embryo immunostaining, zona  
427 pellucida-free injected embryos were fixed with 3.5% paraformaldehyde, permeabilized in 0.5%  
428 Triton X-100 (Sigma) and blocked with 5% BSA and then incubated with primary antibodies against  
429 CDX2 (BioGenex), β-Catenin (1:50, Abcam) and detected by DyLight 549- or 633- conjugated  
430 secondary antibodies(Thermo). Nuclei were stained with DAPI (Sigma). A Nikon-A1 fluorescence  
431 microscope was used for image acquisition.

432

#### 433 **Statistical analysis**

434 Data are presented as mean ± standard error of the mean (SEM). Statistical significance was  
435 determined by Student's *t*-test (two-tail) for two groups or one-way Analysis of Variance (ANOVA)  
436 for multiple groups using Graphpad software. *p* < 0.05 was considered significant.

437

## 438 **Acknowledgments**

439 This work was supported by the National Basic Research Program of China, 973 program grant  
440 2012CB966701, the National Natural Science Foundation of China (NSFC), grant 31171381 (to  
441 J.N.), and core facilities of the Tsinghua–Peking University Center for Life Sciences. TNLIST  
442 Interdisciplinary research foundation grant 042003171 (to Z.X. and N.J.). We thank Dr Danwei  
443 Huangfu for the *AAVS1* homologous recombineering donor plasmids and Dr Xiaohua Shen lab for  
444 assistance in southern blot.

445

## 446 **Author contributions**

447 J.G.: concept and design, collection and/or assembly of data, data analysis and interpretation,  
448 manuscript writing; D.M., R.H., M.Y., J.M.: collection and/or assembly of data; K.K. provided  
449 essential reagents, technical and scientific advice to the experiments and manuscript; Z.X.: concept  
450 and design; J.N.: concept and design, manuscript writing, and final approval of the manuscript.  
451 The authors declare no conflicts of interest.

452

## 453 **Compliance with ethical guidelines**

454 Jianying Guo, Dacheng Ma, Rujin Huang, Jia Ming, Min Ye, Kehkooi Kee, Zhen Xie, and Jie Na  
455 declare that they have no conflict of interest.

456 This article does not contain any studies with human subjects performed by the any of the authors.  
457 All institutional and national guidelines for the care and use of laboratory animals were followed.

458

## 459 **References**

460 Baker DEC, Harrison NJ, Maltby E, Smith K, Moore HD, Shaw PJ, Heath PR, Holden H, and  
461 Andrews PW (2007). Adaptation to culture of human embryonic stem cells and oncogenesis in  
462 vivo. *Nature biotechnology* 25: 207-215

463 Balboa D, Weltner J, Eurola S, Trokovic R, Wartiovaara K, and Otonkoski T (2015). Conditionally  
464 stabilized dCas9 activator for controlling gene expression in human cell reprogramming and  
465 differentiation. *Stem cell reports* 5: 448-459

- 466 Bedzhov I, and Zernicka-Goetz M (2014). Self-organizing properties of mouse pluripotent cells  
467 initiate morphogenesis upon implantation. *Cell* 156:1032-1044
- 468 Boyer LA, Lee TI, Cole MF, Johnstone SE, Levine SS, Zucker JP, Guenther MG, Kumar RM,  
469 Murray HL, and Jenner RG (2005). Core transcriptional regulatory circuitry in human  
470 embryonic stem cells. *Cell* 122: 947-956
- 471 Brons IGM, Smithers LE, Trotter MWB, Rugg-Gunn P, Sun B, de Sousa Lopes SMC, Howlett SK,  
472 Clarkson A, Ahrlund-Richter L, and Pedersen RA (2007). Derivation of pluripotent epiblast  
473 stem cells from mammalian embryos. *Nature* 448: 191-195
- 474 Burridge PW, Holmström A, and Wu JC (2015). Chemically defined culture and cardiomyocyte  
475 differentiation of human pluripotent stem cells. *Current Protocols in Human Genetics*: 21.23.  
476 21-21.23. 15
- 477 Chambers I, Silva J, Colby D, Nichols J, Nijmeijer B, Robertson M, Vrana J, Jones K, Grotewold L,  
478 and Smith A (2007). Nanog safeguards pluripotency and mediates germline development.  
479 *Nature* 450: 1230-1234
- 480 Chang M-Y, Rhee Y-H, Yi S-H, Lee S-J, Kim R-K, Kim H, Park C-H, and Lee S-H (2014).  
481 Doxycycline enhances survival and self-renewal of human pluripotent stem cells. *Stem cell*  
482 *reports* 3: 353-364
- 483 Chavez A, Scheiman J, Vora S, Pruitt BW, Tuttle M, Iyer EPR, Lin S, Kiani S, Guzman CD, and  
484 Wiegand DJ (2015). Highly efficient Cas9-mediated transcriptional programming. *Nature*  
485 *methods* 12: 326-328
- 486 Chen Y, Niu Y, Li Y, Ai Z, Kang Y, Shi H, Xiang Z, Yang Z, Tan T, and Si W (2015). Generation of  
487 cynomolgus monkey chimeric fetuses using embryonic stem cells. *Cell Stem Cell* 17: 116-124
- 488 Deglincerti A, Croft GF, Pietila LN, Zernicka-Goetz M, Siggia ED, and Brivanlou AH (2016).  
489 Self-organization of the in vitro attached human embryo. *Nature* 533: 251-254
- 490 DeKolver RC, Choi VM, Moehle EA, Paschon DE, Hockemeyer D, Meijsing SH, Sancak Y, Cui X,  
491 Steine EJ, and Miller JC (2010). Functional genomics, proteomics, and regulatory DNA  
492 analysis in isogenic settings using zinc finger nuclease-driven transgenesis into a safe harbor  
493 locus in the human genome. *Genome research* 20: 1133-1142
- 494 Duggal G, Warriar S, Ghimire S, Broekaert D, Van der Jeught M, Lierman S, Deroo T, Peelman L,  
495 Van Soom A, and Cornelissen R (2015). Alternative routes to induce naive pluripotency in  
496 human embryonic stem cells. *Stem Cells* 33: 2686-2698

- 497 Gafni O, Weinberger L, Mansour AA, Manor YS, Chomsky E, Ben-Yosef D, Kalma Y, Viukov S,  
498 Maza I, and Zviran A (2013). Derivation of novel human ground state naive pluripotent stem  
499 cells. *Nature* 504: 282-286
- 500 Genga RM, Kearns NA, and Maehr R (2016). Controlling transcription in human pluripotent stem  
501 cells using CRISPR-effectors. *Methods* 101: 36-42
- 502 Gilbert LA, Horlbeck MA, Adamson B, Villalta JE, Chen Y, Whitehead EH, Guimaraes C, Panning  
503 B, Ploegh HL, and Bassik MC (2014). Genome-scale CRISPR-mediated control of gene  
504 repression and activation. *Cell* 159: 647-661
- 505 Gong S, Li Q, Jeter CR, Fan Q, Tang DG, and Liu B (2015). Regulation of NANOG in cancer cells.  
506 *Molecular carcinogenesis* 54: 679-687
- 507 González F, Zhu Z, Shi Z-D, Lelli K, Verma N, Li QV, and Huangfu D (2014). An iCRISPR  
508 platform for rapid, multiplexable, and inducible genome editing in human pluripotent stem  
509 cells. *Cell Stem Cell* 15: 215-226
- 510 Hanna J, Cheng AW, Saha K, Kim J, Lengner CJ, Soldner F, Cassady JP, Muffat J, Carey BW, and  
511 Jaenisch R (2010). Human embryonic stem cells with biological and epigenetic characteristics  
512 similar to those of mouse ESCs. *Proceedings of the National Academy of Sciences* 107:  
513 9222-9227
- 514 Hanna J, Saha K, Pando B, Van Zon J, Lengner CJ, Creighton MP, van Oudenaarden A, and  
515 Jaenisch R (2009). Direct cell reprogramming is a stochastic process amenable to acceleration.  
516 *Nature* 462: 595-601
- 517 Hilton IB, D'Ippolito AM, Vockley CM, Thakore PI, Crawford GE, Reddy TE, and Gersbach CA  
518 (2015). Epigenome editing by a CRISPR-Cas9-based acetyltransferase activates genes from  
519 promoters and enhancers. *Nature biotechnology* 33: 510-517
- 520 Hockemeyer D, Soldner F, Beard C, Gao Q, Mitalipova M, DeKolver RC, Katibah GE, Amora R,  
521 Boydston EA, and Zeitler B (2009). Efficient targeting of expressed and silent genes in human  
522 ESCs and iPSCs using zinc-finger nucleases. *Nature biotechnology* 27: 851-857
- 523 Hogan B, Costantini F, and Lacy E (1986). *Manipulating the mouse embryo: a laboratory manual*,  
524 Vol 34 (Cold spring harbor laboratory Cold Spring Harbor, NY).
- 525 Hsu PD, Lander ES, and Zhang F (2014). Development and applications of CRISPR-Cas9 for  
526 genome engineering. *Cell* 157: 1262-1278

- 527 Kearns NA, Genga RMJ, Enuameh MS, Garber M, Wolfe SA, and Maehr R (2014). Cas9  
528 effector-mediated regulation of transcription and differentiation in human pluripotent stem  
529 cells. *Development* 141: 219-223
- 530 Konermann S, Brigham MD, Trevino AE, Joung J, Abudayyeh OO, Barcena C, Hsu PD, Habib N,  
531 Gootenberg JS, and Nishimasu H (2014). Genome-scale transcriptional activation by an  
532 engineered CRISPR-Cas9 complex. *Nature* 517: 583-588
- 533 Lombardo A, Cesana D, Genovese P, Di Stefano B, Provasi E, Colombo DF, Neri M, Magnani Z,  
534 Cantore A, and Riso PL (2011). Site-specific integration and tailoring of cassette design for  
535 sustainable gene transfer. *Nature methods* 8: 861-869
- 536 Maeder ML, Linder SJ, Cascio VM, Fu Y, Ho QH, and Joung JK (2013). CRISPR RNA-guided  
537 activation of endogenous human genes. *Nature methods* 10: 977-979
- 538 Mandegar MA, Huebsch N, Frolov EB, Shin E, Truong A, Olvera MP, Chan AH, Miyaoka Y,  
539 Holmes K, and Spencer CI (2016). CRISPR Interference Efficiently Induces Specific and  
540 Reversible Gene Silencing in Human iPSCs. *Cell Stem Cell* 18: 541-553
- 541 Mitsui K, Tokuzawa Y, Itoh H, Segawa K, Murakami M, Takahashi K, Maruyama M, Maeda M, and  
542 Yamanaka S (2003). The homeoprotein Nanog is required for maintenance of pluripotency in  
543 mouse epiblast and ES cells. *Cell* 113: 631-642
- 544 Ordovás L, Boon R, Pistoni M, Chen Y, Wolfs E, Guo W, Sambathkumar R, Bobis-Wozowicz S,  
545 Helsen N, and Vanhove J (2015). Efficient recombinase-mediated cassette exchange in hPSCs  
546 to study the hepatocyte lineage reveals AAVS1 locus-mediated transgene inhibition. *Stem cell*  
547 *reports* 5: 918-931
- 548 Qian K, Huang CL, Chen H, Blackburn LW, Chen Y, Cao J, Yao L, Sauvey C, Du Z, and Zhang SC  
549 (2014). A simple and efficient system for regulating gene expression in human pluripotent stem  
550 cells and derivatives. *Stem Cells* 32: 1230-1238
- 551 Shahbazi MN, Jedrusik A, Vuoristo S, Recher G, Hupalowska A, Bolton V, Fogarty NME, Campbell  
552 A, Devito LG, and Ilic D (2016). Self-organization of the human embryo in the absence of  
553 maternal tissues. *Nature cell biology* 18: 700-708
- 554 Silva J, Nichols J, Theunissen TW, Guo G, van Oosten AL, Barrandon O, Wray J, Yamanaka S,  
555 Chambers I, and Smith A (2009). Nanog is the gateway to the pluripotent ground state. *Cell* 138:  
556 722-737
- 557 Smith JR, Maguire S, Davis LA, Alexander M, Yang F, Chandran S, and Pedersen RA (2008).

- 558 Robust, persistent transgene expression in human embryonic stem cells is achieved with  
559 AAVS1-targeted integration. *Stem Cells* 26: 496-504
- 560 Taapken SM, Nisler BS, Newton MA, Sampsell-Barron TL, Leonhard KA, McIntire EM, and  
561 Montgomery KD (2011). Karyotypic abnormalities in human induced pluripotent stem cells  
562 and embryonic stem cells. *Nature biotechnology* 29: 313-314
- 563 Takashima Y, Guo G, Loos R, Nichols J, Ficiz G, Krueger F, Oxley D, Santos F, Clarke J, and  
564 Mansfield W (2014). Resetting transcription factor control circuitry toward ground-state  
565 pluripotency in human. *Cell* 158: 1254-1269
- 566 Tanenbaum ME, Gilbert LA, Qi LS, Weissman JS, and Vale RD (2014). A protein-tagging system  
567 for signal amplification in gene expression and fluorescence imaging. *Cell* 159: 635-646
- 568 Tesar PJ, Chenoweth JG, Brook FA, Davies TJ, Evans EP, Mack DL, Gardner RL, and McKay RDG  
569 (2007). New cell lines from mouse epiblast share defining features with human embryonic  
570 stem cells. *Nature* 448: 196-199
- 571 Theunissen TW, Powell BE, Wang H, Mitalipova M, Faddah DA, Reddy J, Fan ZP, Maetzel D, Ganz  
572 K, and Shi L (2014). Systematic identification of culture conditions for induction and  
573 maintenance of naive human pluripotency. *Cell Stem Cell* 15: 471-487
- 574 Ware CB, Nelson AM, Mechem B, Hesson J, Zhou W, Jonlin EC, Jimenez-Caliani AJ, Deng X,  
575 Cavanaugh C, and Cook S (2014). Derivation of naive human embryonic stem cells.  
576 *Proceedings of the National Academy of Sciences* 111: 4484-4489
- 577 Wiedenheft B, Sternberg SH, and Doudna JA (2012). RNA-guided genetic silencing systems in  
578 bacteria and archaea. *Nature* 482: 331-338
- 579 Xu X, Tao Y, Gao X, Zhang L, Li X, Zou W, Ruan K, Wang F, Xu G-l, and Hu R (2016). A  
580 CRISPR-based approach for targeted DNA demethylation. *Cell Discovery* 2: 16009
- 581 Zhu Z, González F, and Huangfu D (2014). The iCRISPR platform for rapid genome editing in  
582 human pluripotent stem cells. *Methods in enzymology* 546: 215
- 583 Zhu Z, Verma N, González F, Shi Z-D, and Huangfu D (2015). A CRISPR/Cas-mediated  
584 selection-free knockin strategy in human embryonic stem cells. *Stem cell reports* 4: 1103-1111

585

586

## 587 **Figure Legends**

588 **Figure 1. The dCas9-VPR system leads to robust transcription activation in human cell lines.**

- 589 (A) Schematic diagram of the gRNA guided dCas9-VPR gene activation system that consists of  
590 two parts: one plasmid contains dCas9-VPR driven by a CAG promoter; another plasmid  
591 contains gRNA targeting the promoter of the gene of interest driven by the human U6  
592 promoter, in this case gTetO, and a PuroR selection cassette driven by an EF1 $\alpha$  promoter.  
593 Upon co-transfection of the two plasmids, dCas9-VPR can activate the BFP transcription  
594 downstream of the TRE promoter.
- 595 (B) Tet-On system: rtTA protein can bind to the TRE promoter and drive expression of the  
596 down-stream BFP gene in the presence of Dox.
- 597 (C) 293FT cells were transfected with the reporter plasmid containing BFP driven by the TRE  
598 promoter. They were either co-transfected with dCas9-VPR or dCas9-VP64 and gTetO  
599 plasmids, or with the CAG-rtTA plasmid. Dox was added immediately after transfection.  
600 Cells were harvested 2 days after transfection and the fluorescence was analyzed using flow  
601 cytometry.
- 602 (D) Bar graph quantification of mean fluorescent intensity analyzed using the FlowJo software  
603 v7.6.1. \*\*\* $p < 0.001$ , \*\*\*\* $p < 0.0001$ ,  $n = 3$ .
- 604 (E) H9 hESCs were electroporated with either rtTA or dCas9-VPR+gTetO plasmids together with  
605 the TRE-BFP plasmid. Dox was added immediately after electroporation. Cells were harvested  
606 3 days after electroporation and analyzed using flow cytometry.
- 607 (F) Bar graph quantification of the mean fluorescent intensity analyzed using the FlowJo software  
608 v7.6.1. N/A, not applicable. \*\* $p < 0.01$ ,  $n = 2$ .

609

610 **Figure 2. DCas9-VPR can be used to activate single or multiple genes in 293FT cells.**

- 611 (A) *NANOG* gRNA targeting sites were located at -254bp and -144bp upstream of the *NANOG*  
612 transcription starting site (TSS); protospacer-adjacent motif (PAM) sequences in red; black  
613 boxes indicate exons.
- 614 (B) DCas9-VPR and g*NANOG* plasmids were co-transfected into 293FT cells. DCas9-VPR and  
615 gTetO plasmids were used as control. Top panels, fluorescence images of transfected cells;  
616 g*NANOG* plasmid transfected cells showed strong GFP fluorescence. Bottom panel, flow  
617 cytometry analysis of GFP<sup>+</sup> cells in each group.
- 618 (C) Q-PCR analysis of *NANOG* expression 2 days after transfection; the dCas9-VPR system  
619 showed nearly 150-fold up-regulation of *NANOG* mRNA. Relative gene expression values  
620 were normalized against *GAPDH*. Error bars represent SEM. \*\* $p < 0.01$ ,  $n = 3$ .
- 621 (D) Activation of endogenous genes by dCas9-VPR. DCas9-VPR was co-transfected with gRNA  
622 pairs targeting *HOXA10*, *SNAIL1*, *MESPI*, *GATA5* or *HOXA9*, respectively. Cells were

623 harvested 2 days after transfection and subjected to Q-PCR analysis. All tested genes showed  
624 significant upregulation compared to the control group. All expression levels were  
625 normalized against *GAPDH*. Error bars represent SEM. \* $p < 0.05$ , \*\* $p < 0.01$ , \*\*\* $p < 0.001$ ,  
626 \*\*\*\* $p < 0.0001$ ,  $n=3$ .

627 (E) Simultaneously activation of multiple endogenous genes in 293FT cells. DCas9-VPR was  
628 co-transfected with 2×gRNAs (gMESP1, gGATA5), 3×gRNAs (gHOXA10, gSNAIL1,  
629 gHOXA9) or 5×gRNAs (gHOXA10, gSNAIL1, gMESP1, gGATA5 and gHOXA9). Cells  
630 were harvested 2 days after transfection. Q-PCR analysis confirmed co-upregulation of  
631 multiple genes targeted by pooled gRNAs. All expression levels normalized against *GAPDH*.  
632 Error bars represent SEM. \* $p < 0.05$ , \*\* $p < 0.01$ , \*\*\*\* $p < 0.0001$ ,  $n=3$ .

633

### 634 **Figure 3. Activation of endogenous *NANOG* gene in hESCs by dCas9-VPR.**

635 (A) Immunostaining showing upregulation of NANOG protein by the dCas9-VPR system. Cells  
636 were fixed 5 days after transfection. WT Ctrl, untransfected H9 cells; Diff, differentiated H9  
637 cells induced by 10  $\mu$ M retinoic acid (RA); gNANOG, H9 cells co-transfected with  
638 dCas9-VPR and gNANOG plasmids; *NANOG* CDS, cells co-transfected with CAG-rtTA and  
639 TRE driving *NANOG*-2A-H2B-mCherry. Dox were added immediately after electroporation.  
640 All plasmids were based on the PiggyBac system and co-transfected with a plasmid  
641 containing HyperPB transposase driven by a CAG promoter. Scale bar, 20  $\mu$ m.

642 (B) Q-PCR analysis of *NANOG* and *OCT4* expression in H9 cells 5 days after transfection. All  
643 expression levels normalized against *GAPDH*. Error bars represent SEM. \* $p < 0.05$ ,  $n=3$ .

644 (C) Western blot analysis of *NANOG* and *OCT4* protein expression in H9 hESCs. Cells were  
645 harvested 5 days after transfection without selection.

646 (D) DCas9-VPR constitutive expressing H9 cells showed similar clone morphology after long-term  
647 culture. Scale bar, 100  $\mu$ m.

648 (E) Q-PCR result showing dCas9-VPR constitutive expressing H9 cells and wild-type H9 cells  
649 expressed similar amount of *NANOG*. All expression levels normalized against *GAPDH*. Error  
650 bars represent SEM. ns.  $p > 0.05$ , \*\*\* $p < 0.001$ ,  $n=3$ .

651

### 652 **Figure 4. Generation of the iVPR hESC line.**

653 (A) Schematic view of wild type, targeted *AAVS1* locus, and positions of southern blot probes. B  
654 (Bgl II site), S (Sph I site), EXT (external probe), INT (internal probe). The sizes of the  
655 expected bands are indicated at the top. Blue lines indicate homology to the *PPP1R12C*

- 656 intron. HA-L and HA-R, left and right homology arms.
- 657 (B) Southern blot confirmed the correct targeted *AAVS1* locus in the iVPR clone 2#, 6#, 8#. M,  
658 marker.
- 659 (C) Q-PCR analysis of dCas9-VPR transcript levels with or without Dox treatment. Expression  
660 levels were normalized against *GAPDH*. Error bar represents SEM.
- 661 (D) Western blot of dCas9-VPR protein level upon Dox addition and after Dox withdrawal in  
662 idCas9-VPR clone 2. The time points are indicated at the top.
- 663 (E) Q-PCR showing that the induction of *dCas9-VPR* was not affected by differentiation. Cells  
664 were induced to undergo mesoderm differentiation for 3 days in the presence or absence of  
665 Dox. Gene expression levels were all normalized against *GAPDH*. Error bar indicates SEM.  
666 \*\*\* $p < 0.001$ , \*\*\*\* $p < 0.0001$ ,  $n=3$ .

667

668 **Figure 5. Upregulation of *NANOG* by dCas9-VPR promoted clonogenicity and the naïve state**  
669 **of pluripotency.**

- 670 (A) Q-PCR analysis of *NANOG* upregulation in iNANOG cells. iVPR clones 2, 6, and 8 were  
671 electroporated with gRNA expression plasmid targeting the *NANOG* promoter, as shown in  
672 Fig. 2A. GFP positive cells were purified by FACS and maintained as iNANOG cells. They  
673 were treated with or without Dox (1  $\mu\text{g/ml}$ ) for 2 days. *NANOG* expression level was  
674 normalized against *GAPDH*. Error bar represents SEM. *NANOG* expression level  
675 significantly elevated only in iNANOG+Dox group.  $n=3$ .
- 676 (B) Q-PCR analysis of *NANOG* down-regulation in iNANOG cells. Dox was added for 2 days,  
677 then removed. Cells were harvested at different time points, as indicated. *NANOG* expression  
678 was normalized against *GAPDH*. Error bar represents SEM. *NANOG* expression level  
679 significantly dropped during Dox withdraw.  $n=3$ .
- 680 (C) Western blot showing increased *NANOG* protein expression in iNANOG cells at different  
681 time points after Dox treatment. SE, short exposure; LE, long exposure; d, day; h, hour.
- 682 (D) Western blot showing *NANOG* protein expression decrease in iNANOG cells at different time  
683 points after Dox withdrawal. SE, short exposure; LE, long exposure; d, day; h, hour.
- 684 (E) Q-PCR analysis showing upregulation of pluripotency gene *OCT4*, *PRDM14*, *GDF3*, and  
685 *LEFTYB*, and down-regulation of differentiation gene *AFP*. Expression level all normalized  
686 against *GAPDH*. Error bar represents SEM. N/A, not applicable. ns.  $p > 0.05$ , \* $p < 0.05$ , \*\* $p <$   
687  $0.01$ , \*\*\* $p < 0.001$ , \*\*\*\* $p < 0.0001$ ,  $n=3$ .
- 688 (F) Q-PCR analysis showing downregulation of *XIST* after *NANOG* induction. Expression level  
689 normalized against *GAPDH*. Error bar represents SEM. ns.  $p > 0.05$ , \* $p < 0.05$ ,  $n=3$ .

- 690 (G) Flow cytometry analysis showing increased SSEA3 expression after *NANOG* induction. Data  
691 analyzed using the FlowJo software v7.6.1.
- 692 (H) Clonogenicity assay of iNANOG cells. Alkaline phosphatase assay (dark blue) was used to  
693 visualize undifferentiated colonies.
- 694 (I) Bar graph quantification of the clonogenicity assay. ns.  $p > 0.05$ ,  $*p < 0.05$ ,  $n=3$ .
- 695 (J) Morphology of iNANOG cells cultured in the 2iL medium. *NANOG* overexpression  
696 (iNANOG + Dox) promoted long-term cell growth in the 2iL medium. Representative images  
697 of passages 1 and 8 (P1 and P8) are shown. Scale bar, 100  $\mu\text{m}$ .
- 698 (K) Morphology of primed state iNANOG cells (without Dox) and Dox induced iNANOG cells  
699 (passage 9, P9) in the 2iL medium.
- 700
- 701 **Figure 6. Upregulation of *NANOG* by idCas9-VPR promoted hESC survival and ICM**  
702 **integration in mouse blastocysts *in vitro*.**
- 703 (A) Cartoon showing *in vitro* hESC-mouse blastocyst chimera formation assay. iNANOG cells  
704 were cultured in E8 or 2iL/FK medium with or without Dox, then injected into E3.5 mouse  
705 blastocysts and cultured to E4.5 in KSOM: 2iL/FK = 1:1 medium *in vitro*.
- 706 (B) Morphology of iNANOG cells in culture and chimeric embryos. Top 2 rows, cells cultured in  
707 E8 or 2iL/FK on feeders; scale bar, 100  $\mu\text{m}$ . Bottom 2 rows, E3.5 and E4.5 mouse blastocysts  
708 with iNANOG cells (GFP); scale bar, 100  $\mu\text{m}$ .
- 709 (C) Survival curve of hESC in mouse blastocysts over time. WTSG, wild type hESCs expressing  
710 *NANOG* gRNA. The  $p$  value was calculated using the Log-rank (Mantel-Cox) test. ns.  
711  $p > 0.05$ ,  $*p < 0.05$ ,  $***p < 0.001$ . Detailed information is provided in Fig. S4B.
- 712 (D) Confocal images of E4.5 chimeric embryos.  $\beta$ -Catenin, yellow; CDX2, red; DNA, blue;  
713 iNANOG cells, green. The ICM region is highlighted by a dashed circle. Scale bar, 20  $\mu\text{m}$ .
- 714 (E) Selected frame from time-lapse movie of iNANOG-mouse blastocyst chimera. Arrows  
715 indicating iNANOG cells moved with mouse inner cell mass cells during blastocyst hatching.  
716 Scale bar, 100  $\mu\text{m}$ .
- 717 (F) The proportion of blastocysts with hESC integration for E4.5 embryos. Blastocysts with GFP  
718 cells in both ICM and TE were counted as ICM. The percentage of embryos with  
719 ICM/TE/None integration was labeled in the colored bar.
- 720 (G) Dot graph showing the number of iNANOG cells in the ICM region of E4.5 embryos. Cells,  
721 culture condition before injection, and number of embryos were as listed. Error bars represent  
722 SEM. ns.  $p > 0.05$ ,  $**p < 0.01$ .

**Figure 1**

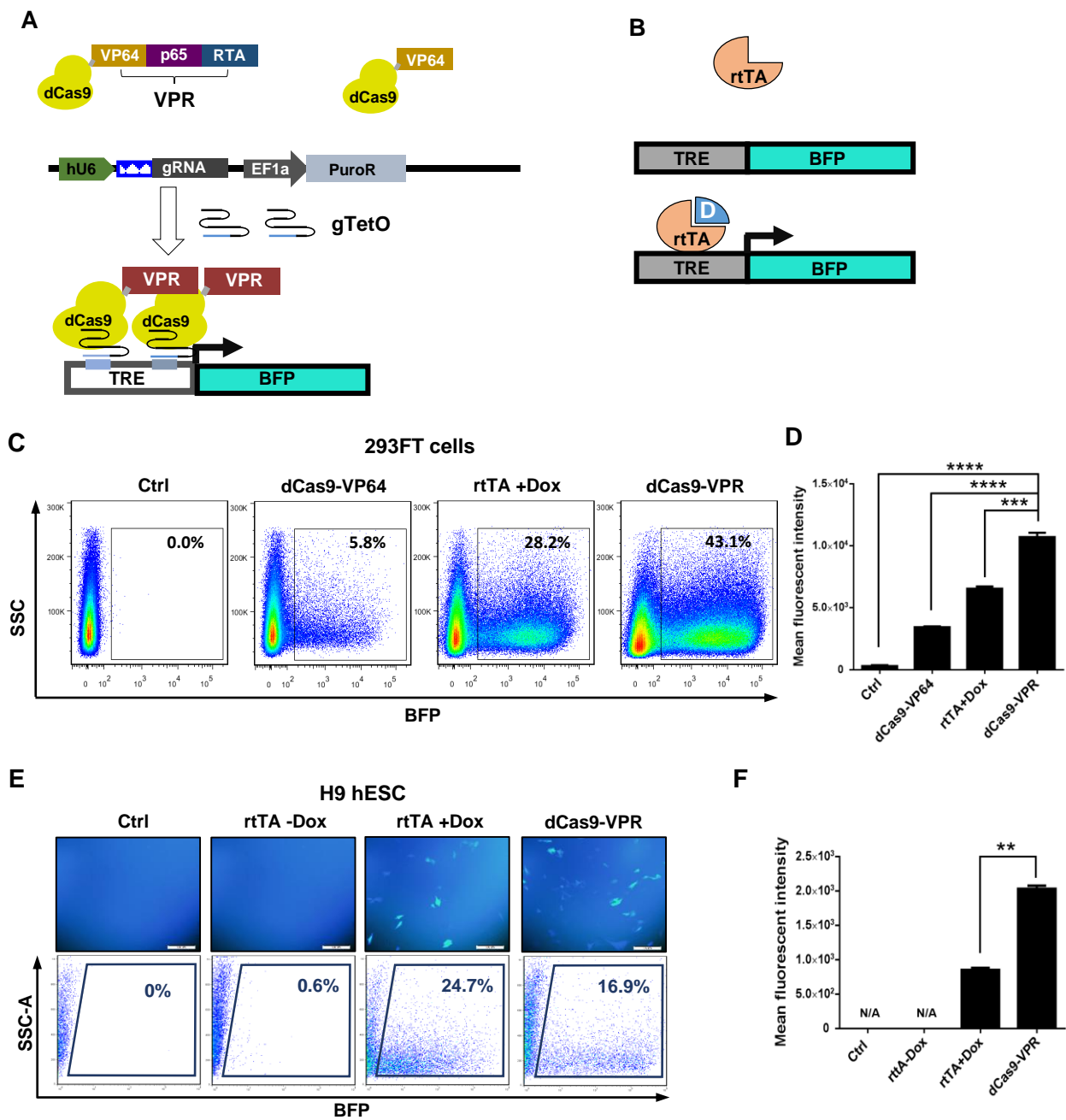


**Figure 2**

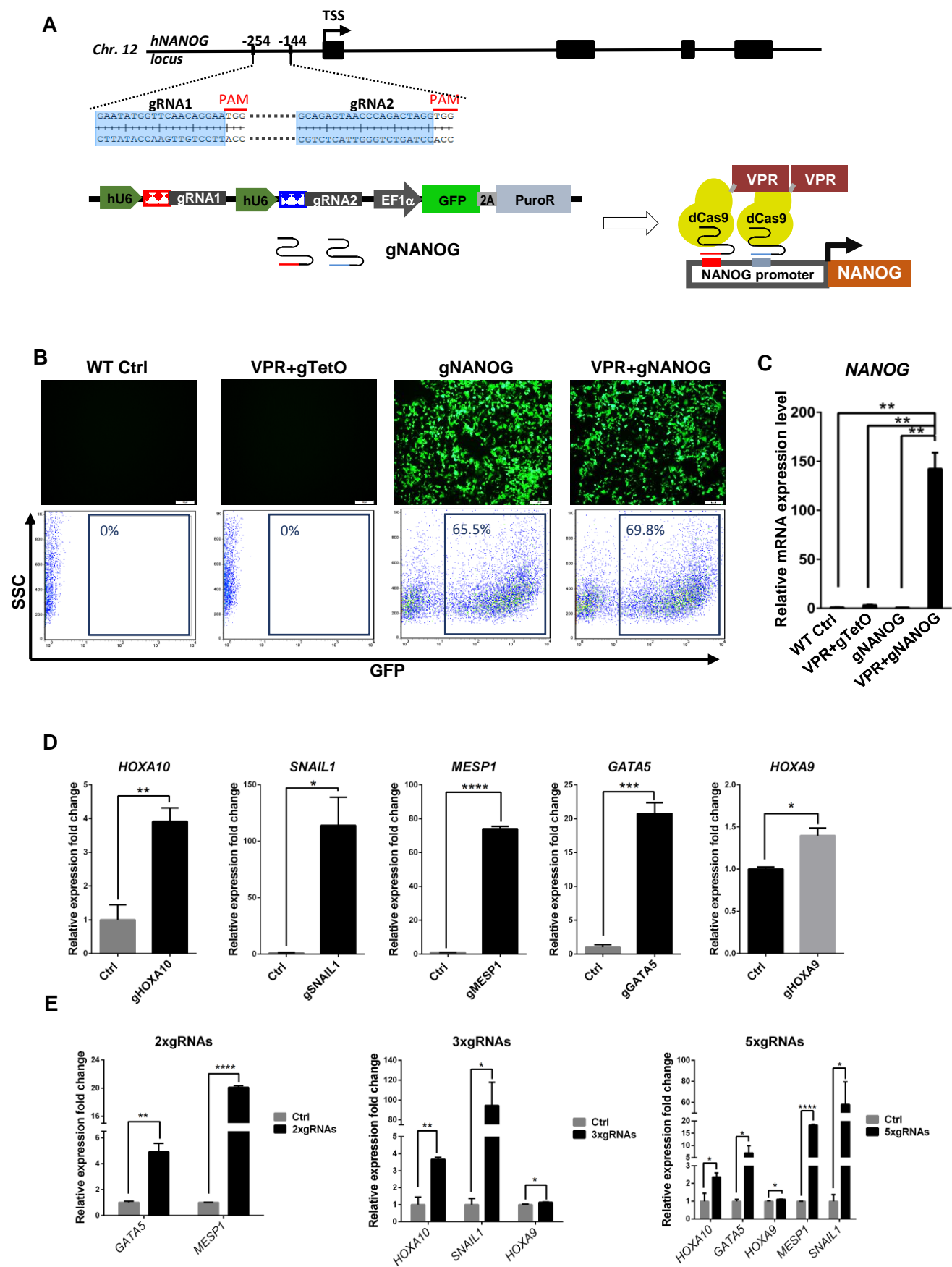


### Figure 3

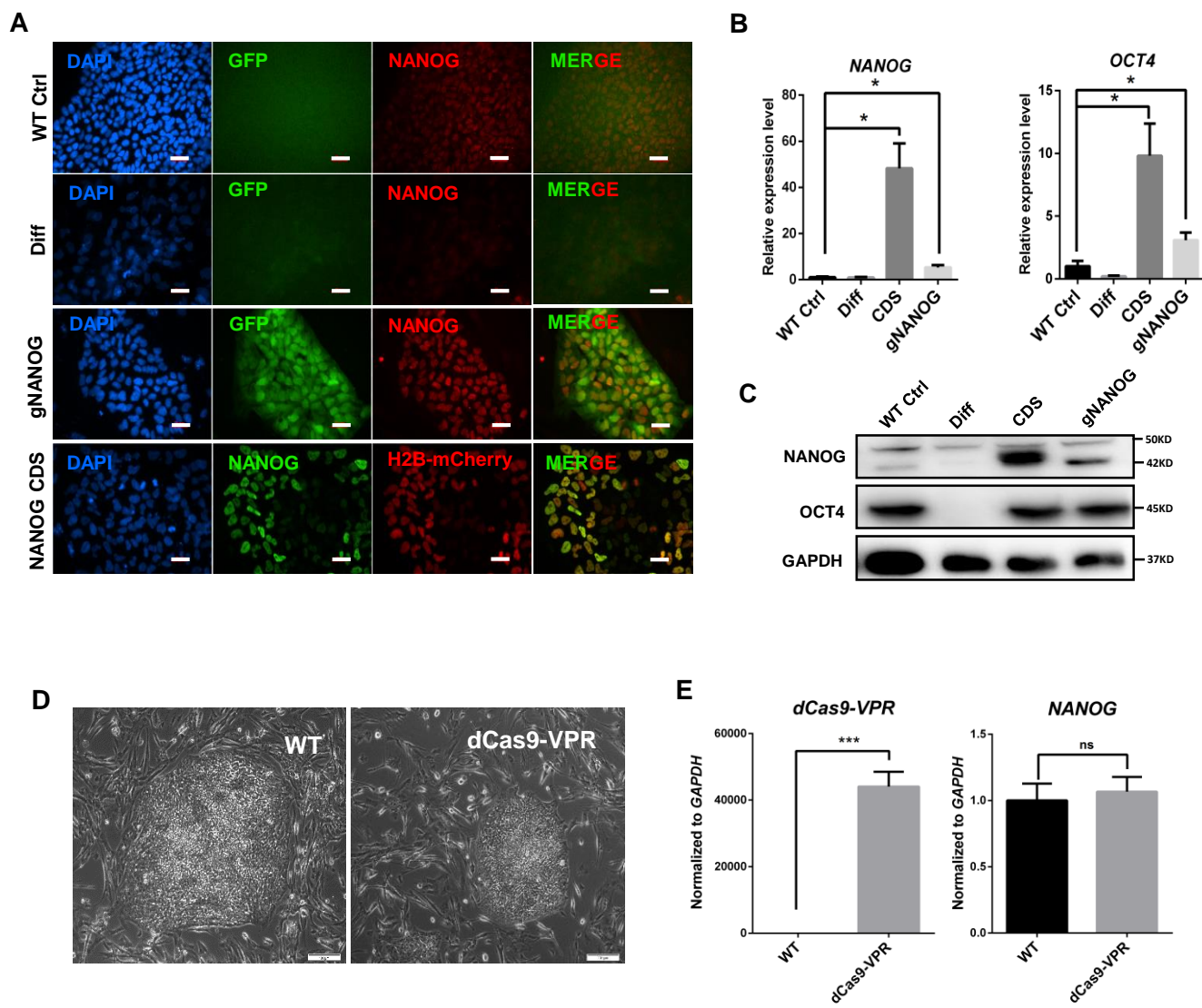


**Figure 4**

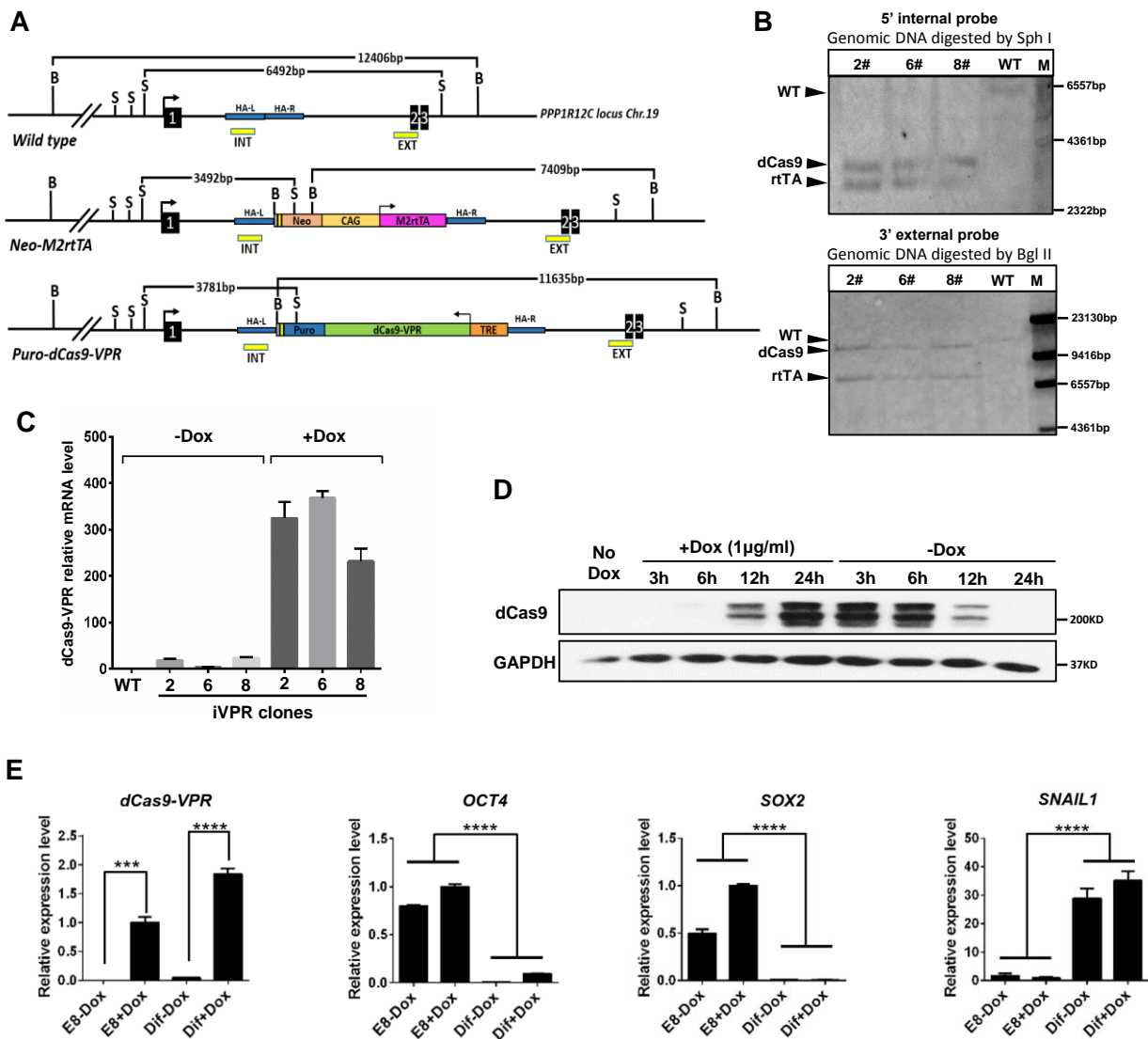


**Figure 5**

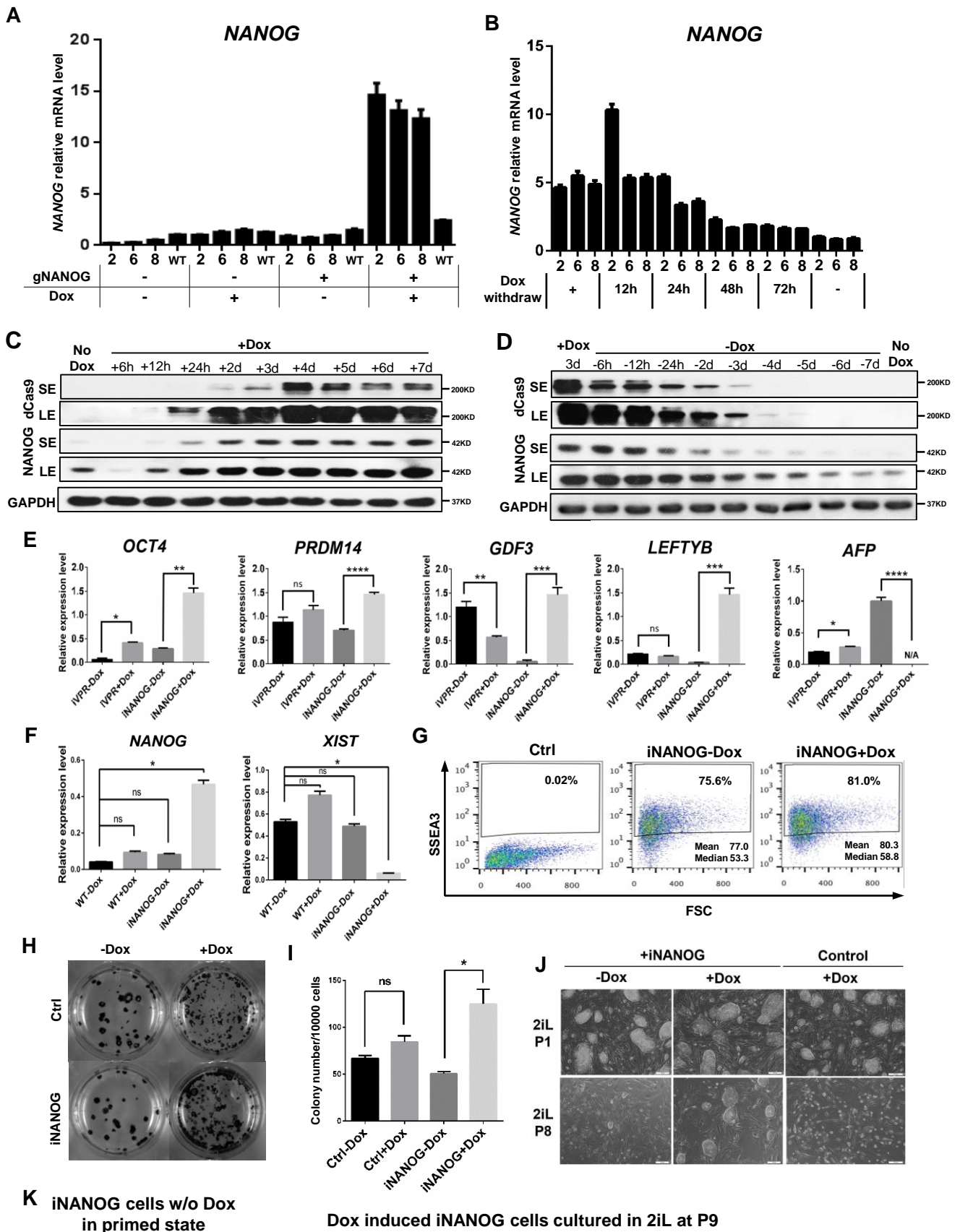


**Figure 6**

